



Numerical Study of Water-air Ejector using Mixture and Two-phase Models

M. R. Assari^{*a}, H. Basirat Tabrizi^b, A. Jafar Gholi Beik^a, K. Shamesri^a

^a Department of Mechanical Engineering, Jundi-Shapur University of Technology, Dezful, Iran

^b Department of Mechanical Engineering, Amirkabir University of Technology, Tehran, Iran

PAPER INFO

Paper history:

Received 22 July, 2021

Received in revised form 14 October 2021

Accepted 16 October 2021

Keywords:

Liquid-gas Ejector

Two-phase Flow

Mixture Method

Eulerian-Eulerian Method

Numerical Simulation

ABSTRACT

In this research, steady-state Mixture and Eulerian-Eulerian method for liquid-gas parallel flow ejector were examined. The simulation demonstrated that the Mixture model simulation represents better and efficient. The Eulerian-Eulerian model needed longer computational time and had a complexity to achieve the optimal convergence. However, both methods' performances were shown slightly similar. The models indicated a difference of about 6% in the flow rate ratio, their pressure diagrams nearly coincide, and their velocity parameter varies by 7% by comparing to the existing experimental data. Additionally, the Mixture model results appropriately conformed much better to the experimental data. So, the Mixture model was chosen for further parametric study. Simulation results indicated that the flow rate ratio decreases by increasing the throat's cross-sectional area, and the flow rate ratio increases by increasing the nozzle's cross-sectional area. In this regard, e.g., the flow rate ratio of ejector by increasing pressure from 70 to 80 kPa, the air inlet increases up to 94%, and by increasing ejector outlet pressure, the flow rate ratio reduces such that no suction can be observed at 160 kPa. Consequently, at 150 kPa pressure ratio, the flow rate ratio was reduced by almost 100%.

doi: 10.5829/ije.2022.35.02b.06

NOMENCLATURE

Model coefficients	c	-	Stress	τ	$\frac{N}{m^2}$
Generation of turbulence	G	-	Turbulent Schmidt number	σ	-
Turbulence kinetic energy	k	$\frac{m^2}{s^2}$	Turbulent Prandtl number	σ	-
Pressure	P	Pa	Model coefficients	$\sigma_k, \sigma_\epsilon$	-
Source	S	$\frac{kg}{s.m^3}$	Kinetic energy dissipation	ϵ	$\frac{m^2}{s^3}$
Strain rate	S_{IJ}	$\frac{1}{s}$	dynamic viscosity	μ	Pa.s
Velocity	u	$\frac{m}{s}$	Kinetic viscosity	ν	Pa.s
Fluctuating velocity	\dot{u}	$\frac{m}{s}$	Subscript Symbols		
Position	x	m	Vector / Types	i, j, k	
Contribution of the fluctuating dilatation	Y	-	Turbulence	t	
Volumetric fraction	α	-	Effective	eff	
Density	ρ	$\frac{kg}{m^3}$	Phase	q	

*Corresponding Author Institutional Email: Assari@jsu.ac.ir (M. R. Assari)

1. INTRODUCTION

Nowadays, there are a wide range of engineering research area, which can not be assessed, only by means of experiments. Computational Fluid Dynamic (CFD) is a suitable tool to investigate many engineering problems, e.g. aerodynamic [1], cavitation [2], hydraulic [3, 4], energy systems [5, 6], heat transfer [7, 8], multiphase flow [9-11]. Today, two-phase ejectors are highly efficient and widely applied in various industries. Ejectors are categorized into two types of constant-pressure and constant-area depending on the nozzle exit position (NXP) of the ejector. If the nozzle exit is located in the constant-pressure mixing chamber, the ejector is pressure-constant. On the other hand, if the nozzle exit is placed in the constant-area, the ejector is of constant-area type. The ejector with constant pressure was initially proposed by Keenan et al. [12]. Although the constant-area ejector can create a higher suction mass flow rate, the constant-pressure ejector is considered more appropriate since it provides a greater backpressure range. The liquid-gas ejector includes a nozzle, a suction chamber, a throat, and a diffuser. The shock in ejectors occurs in the constant-area throat. Through this, the flow velocity instantly decreases; afterward, a higher mixing rate is achieved as the two-phase flow passes the diffuser [13]. The mixing flow behavior in two-phase ejectors is highly complex; thus, it cannot be simply described through theoretical and experimental methods [14-16].

CFD is a proper approach, as a research tool, for investigating a liquid-gas ejector's performance [17]. The ejector nozzle is critically significant due to the creation of a partial vacuum in the ejector. In a study by Zhu [18], a nozzle type with a circular geometry was proposed at the primary nozzle throat section. In cases that the ejector geometry is constant, changing the ejector operating conditions will also have a significant impact on its performance. Moreover, according to Zhu and Li [19], mixing chamber considerably affects the ejector performance. The convergence angle was reported 6° and -8° , as well as values of 1.45° and -2.4° were achieved, 28° was acquired in Chong and Liu [20], and approximately 6° reported by Kouhikamali and Sharifi [21]. The mentioned differences in obtaining convergence angles correspond to some other aspects: type of ejector, working fluid, and operation.

Wang and Li [22] examined the primary nozzle geometry impression on the ejector performance by simulating computational fluid dynamics. The process was carried out by considering various geometries, including the mixing chamber's convergence angle and the divergent diffuser, the length of the diffuser's divergent section, the throat length, and the wall surface roughness. Among these geometric parameters, it has been noted that the throat and divergent sections of the

nozzle have a significant impression on the flow rate ratio. The ejector performance was sorted into three modes: critical mode, subcritical mode, and back-flow. In the sub-critical mode, a constant and appropriate flow rate ratio was observed. The back pressure increases to a certain amount, critical back pressure will not make an impression, and the flow rate ratio initiates reduction by increasing back pressure.

According to the above literature review, this research has been initially attempted to investigate the impression of ejector modeling using computational fluid dynamics and suggested two multiphase flow modeling, which is Mixture and Eulerian-Eulerian approaches. After examining and comparing with existed similar studies, the Mixture model was chosen as an efficient two-phase flow model. Subsequently, the effects of throat cross-section, nozzle exit, inlet, outlet, and secondary pressures in the liquid ejector are investigated and discussed.

2. MODELING

The corresponding liquid-gas ejector includes two inlets and one outlet. One of the inlets is water with a density and viscosity of $998.2 \frac{kg}{m^3}$ and $0.001003 \frac{kg}{m.s}$, respectively. The other inlet is gas (air) with a density and viscosity of $1.225 \frac{kg}{m^3}$ and $1.7894 \times 10^{-5} \frac{kg}{m.s}$,

respectively. The outlet is a Mixture of air and water, and the utilized ejector is symmetrical about the x-axis. The liquid-gas test model's geometrical dimensions are shown in Figure 1, and the ejector's length is 1 meter. In this study, the two-dimensional axial symmetry is utilized to model and analyze the ejector's flow.

Two Mixture and Eulerian-Eulerian-Eulerian multiphase flow models are considered for identical operating conditions in the simulation process of the liquid-gas parallel flow ejector. The simulation is performed under steady-state conditions, and the flow is assumed incompressible, turbulent, and two-dimensional axially symmetric. The Realizable K- ϵ model is applied for the turbulence model (see Figure 2).

In the Appendix, Table A, the governing equations are displayed. Moreover, independency of the computational grid is a crucially significant step in the simulations. In the present study as shown in Figure 3,

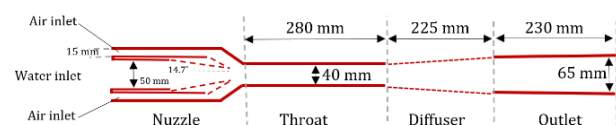


Figure 1. Exact geometry and dimensions of the ejector

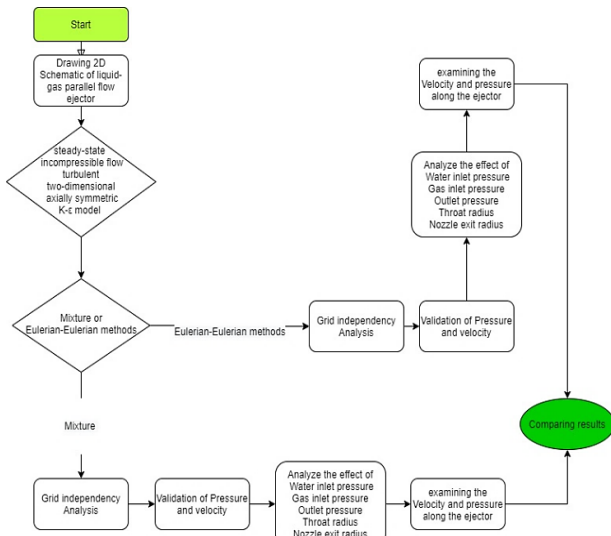


Figure 2. Flowchart of modelling

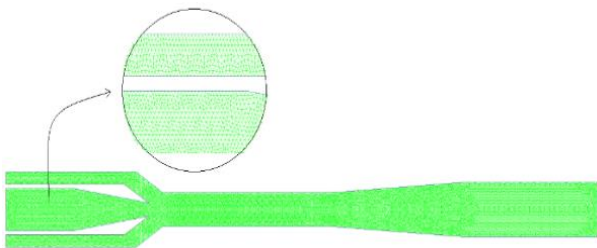


Figure 3. Ejector's grid

three mesh numbers of 12517, 15066, and 20150 were compared in both Mixture and Eulerian-Eulerian methods.

In both methods, no considerable changes were observed in the results. Therefore, the 20150-mesh number was considered for higher accuracy and better convergence.

The simulation results were obtained through a computer with the configurations of 2.50 GHz CPU and 8 GB of RAM. The solution time using the Eulerian-Eulerian method is about 4 hours, and it is reduced to about 3 and a half hours using the Mixture method. Examining grid independency in the simulation process is highly significant. The ejector's pressure and velocity for both methods were examined and validated as shown in Figure 4 and Table 1.

The solution is also reiterated to achieve convergence. The convergence criterion is where the gas flow rate from the secondary inlet becomes constant, and the remainder of each equation completely reaches below $10e-4$.

The longer duration of the Eulerian-Eulerian solution is due to its higher complexity and the higher number of solved equations in comparison to the

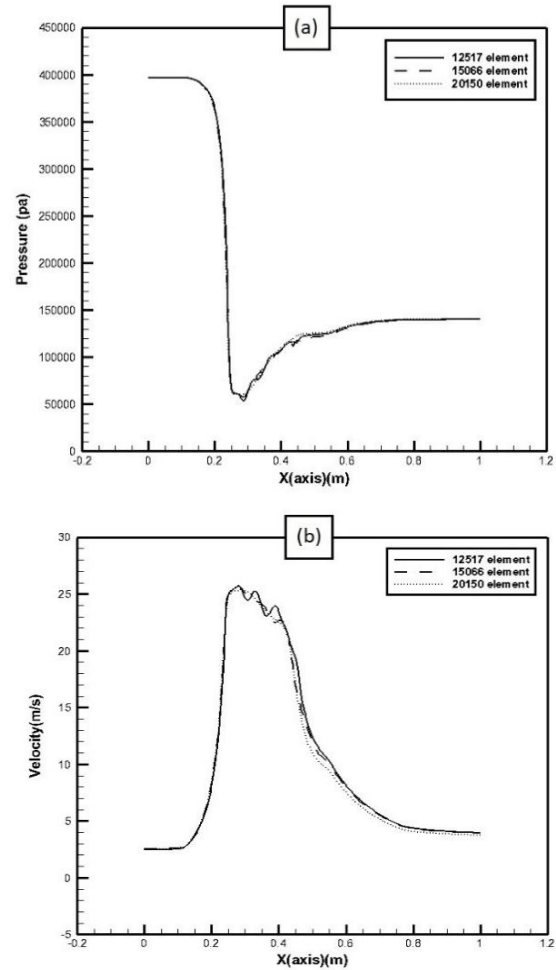


Figure 4. Mesh independency for Mixture Model, (a) pressure, (b) velocity

TABLE 1. Mesh analysis

Mesh size	Profile	Max. mesh error 12517 relative to mesh 15066	Max. mesh error 15066 relative to mesh 20150
Mixture Model	Pressure	2%	0.5%
	Velocity	4%	1.5%
Eulerian-Eulerian Model	Pressure	2%	1%
	Velocity	3.5%	1%

Mixture method. Consequently, the Eulerian-Eulerian method requires greater duration than the Mixture method to obtain the optimal convergence.

In the Mixture method, a second-order discretization method has been applied for momentum and turbulence kinetic energy, and the first-order discretization method has been exploited for volume fraction. Nevertheless, to acquire a solution of optimal convergence through the

Eulerian-Eulerian method, the first-degree discretization method was initially applied for momentum, turbulence kinetic energy, and volume fraction. After reaching relative stability in the solution, the method was changed to a second-order discretization method for momentum and turbulence kinetic energy. However, the first-order discretization method was still utilized for volume fraction. Additionally, the Flow courant number reduced to 20, and the under-relaxation factor for volume fraction was reduced to 0.5. Furthermore, the couple method was used for pressure and velocity coupling. The longer duration of the Eulerian-Eulerian solution is due to its higher complexity and the higher number of solved equations in comparison to the Mixture method. Consequently, the Eulerian-Eulerian method requires greater duration than the Mixture method to obtain the optimal convergence. In the Mixture method, a second-order discretization method has been applied for momentum and turbulence kinetic energy, and the first-order discretization method has been exploited for volume fraction. Nevertheless, to acquire a solution of optimal convergence through the Eulerian-Eulerian method, the first-degree discretization method was initially applied for momentum, turbulence kinetic energy, and volume fraction. After reaching relative stability in the solution, the method was changed to a second-order discretization method for momentum and turbulence kinetic energy. However, the first-order discretization method was still utilized for volume fraction. Additionally, the Flow courant number reduced to 20, and the under-relaxation factor for volume fraction was reduced to 0.5. Furthermore, the couple method was used for pressure and velocity coupling.

In Table 2, the geometric parameters and utilized boundary conditions have been presented, which are a total of 22 cases. In each related part of the examined parameter, the corresponding simulation number in the script is mentioned. The inlet pressure of the ejector for water and gas (air) and outlet are shown in table, and the wall boundary conditions have been considered for the ejector wall.

3. VALIDATION

Simulation results were compared with the obtained experimental data and numerical results of similar studies to evaluate the accuracy of this numerical study. It must be noted that the suction flow rate is regarded as one of the most significant parameters in determining the liquid ejector's performance. Therefore, obtained numerical results are presented along with the experimental data of Bhutada and Pangarkar [23], Cai's [24] and the results of Wang's numerical research [25]. Figure 5 shows comparison of Eulerian-Eulerian

TABLE 2. Geometric parameters and conditions

Simulation conditions	Water inlet pressure (kPa)	Gas (air) inlet pressure (kPa)	Outlet pressure (kPa)	Throat radius (mm)	Nozzle exit radius (mm)
1-4	390	60	140	20	8
	400				
	410				
	420				
5-8	400	50	140	20	8
		60			
		70			
		80			
9-12	400	60	130	20	8
			140		
			150		
			160		
13-17	400	60	160	19	8
				19.5	
				20	
				20.5	
				21	
18-22	400	60	160	7	8
				7.5	
				8	
				8.5	
				9	

Method which indicates a good agreement and similar trend. Further, the suction flow ratio and the pressure ratio comparison with reported data in literature [24, 25] are illustrated in Table 3.

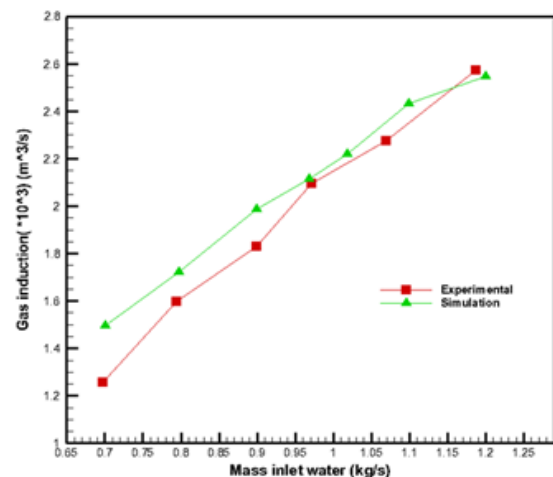


Figure 5. Comparison of Eulerian-Eulerian Method with Bhutada and Pangarkar [23]

TABLE 3. Validation

Flow rate ratio	Pressure ratio of simulation	Pressure ratio, Exp. [24]	Exp. error %	Pressure ratio [25]	Simulation [25] %
0.0245	0.287	0.272	5.5	0.286	0.6
0.173	0.275	0.261	5.3	0.281	1.8
0.371	0.270	0.247	8.5	0.276	2
0.494	0.269	0.238	11.5	0.271	0.7
0.687	0.267	0.224	16.1	0.267	0

As can be observed, the maximum error is 16.1% for the flow rate ratio. The pressure ratio decreases by increasing the flow rate ratio. In Equations (1) and (2), the flow rate ratio and the ejector pressure ratio are represented, respectively:

$$\text{Flow rate ratio} = \frac{Q_{gas}}{Q_{water}} \tag{1}$$

$$\text{Pressure ratio} = \frac{P_{outlet} - P_{gas(air)inlet}}{P_{waterinlet} - P_{gas(air)inlet}} \tag{2}$$

The solution methods of two-phase flow in problem modeling are shown in Figure 6. It can be observed in these figures, the velocity and pressure along the ejector using the Mixture and Eulerian-Eulerian models, as well as the flow rate ratio. According to Figure 6 the most considerable difference is identified in the velocity, and the pressure, which both models nearly similar. The difference reaches about 7% in the velocity profile. Moreover, if they are compared based on a similar output, the flow rate ratio in the Eulerian-Eulerian, and Mixture models will be 1.3217 and 1.2394, respectively, under identical operating conditions. In this regard, the Eulerian-Eulerian model has increased by about 6.23% compared to the Mixture model. Further, as can be seen in the velocity and pressure diagrams, the highest difference has occurred during the velocity reduction and the pressure increase, around 300 mm.

Moreover, Figure 7 shows the velocity contour for the Mixture and Eulerian-Eulerian models. The pressure of water inlet, gas (air) inlet, and outlet are taken 400, 60, and 140 kPa, respectively, as stated in Table 2. As can be observed in both the velocity diagram and the ejector velocity contour, the Mixture model's velocity is lower than the Eulerian-Eulerian model in the constant-area section of the ejector's end. On the other hand, the Eulerian-Eulerian model velocity is lower in the throat section. Due to the proximity of the Mixture model obtained results and time-saving purposes, the Mixture model has been used for other parameters examination.

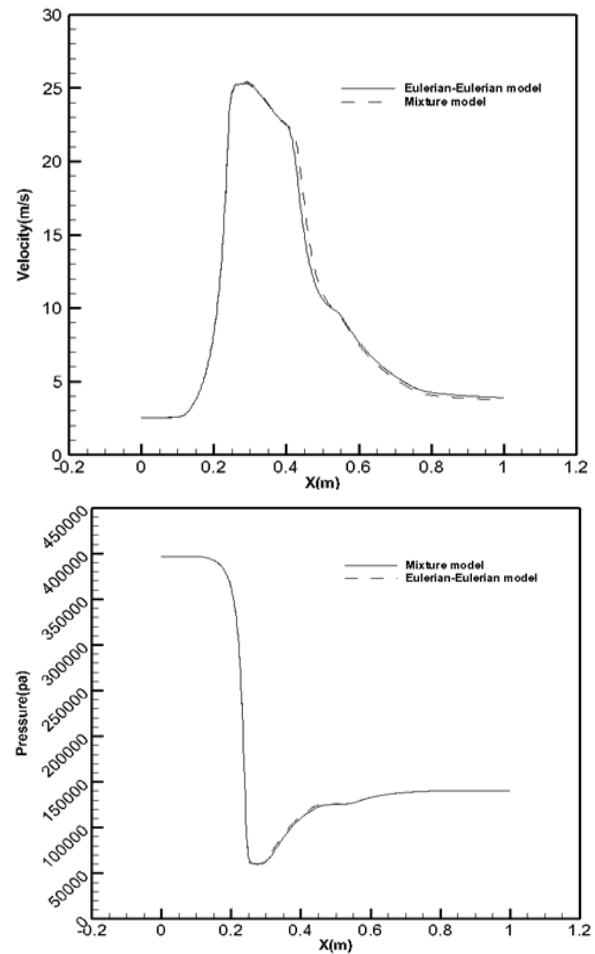


Figure 6. Comparison of a) velocity and b) pressure in Mixture and Eulerian-Eulerian methods

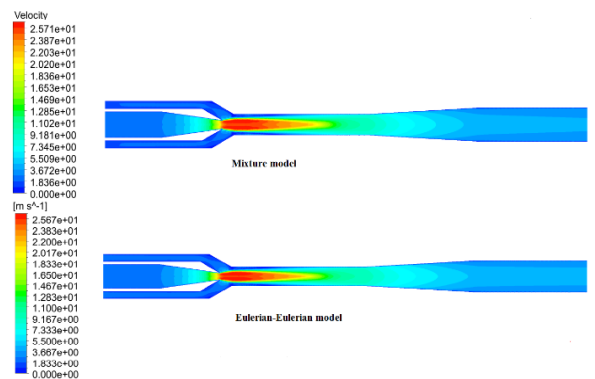


Figure 7. Pressure along the ejector for different the solution method

4. RESULTS AND DISCUSSION

As stated in Figure 8, the water velocity increases after its entry and passing through the nozzle. This velocity increase reduces the pressure at the nozzle exit that

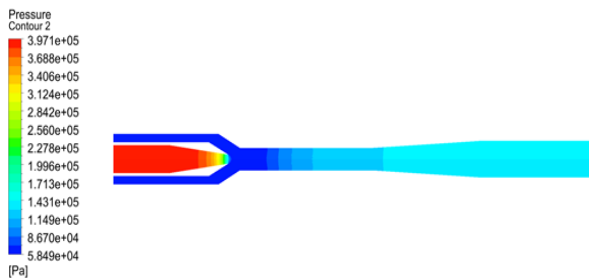


Figure 8. Pressure along the ejector for different the solution method

creates a partial vacuum, which is detectable in Figure 7 for the pressure contour. This pressure reduction causes the secondary fluid (air) suction. After the mixing process in the mixing chamber, the air passes through the constant-area section with a slight velocity decrease; afterward, its velocity decreases. Moreover, in the diffuser, the velocity decreases, and the pressure slightly increases.

Inlet air pressure parameter influentially contributes to the ejector performance. In Figure 9, the inlet air pressure effect on the water phase distribution along the symmetry axis has been displayed. As the inlet air pressure increases, the air momentum amount and its penetration power through the primary water fluid will increase. Additionally, it will affect the water and air phase distribution along the axis. The water volume fraction will decrease by increasing air inlet pressure along the axis. Moreover, the water primary layer's dispersion rate increases while its continuity decreases. The air presence within the water layer will gradually increase along the axis as the axial distance increases. As shown in Figure 9, increasing air inlet pressure from 50 to 60 to 70 and 80 kPa, the volume fraction of water at the center of the ejector's output decreases by 14.6%, 21.03%, and 15.22%, respectively. The flow enters the ejector's entry in the form of two flows and subsequently, the two flows are combined with a part of the airflow at the end of the water primary nozzle exit, which causes the air suction. Afterward, they are passing as a single fluid. The fluid velocity increases by increasing the inlet air pressure; this will change the mixing percentage of two fluids of the flow. Thus, the water volume fraction decreases, and the air volume fraction increases by increasing the inlet air pressure along the axis.

In Figure 10, the distribution of water velocity at different inlet pressures is demonstrated. As pressure increases, the primary fluid velocity increases; thus, higher momentum of primary fluid can be observed at the output. Through the air inlet pressure increase from 50 to 60, 60 to 70, and 70 to 80 kPa, the outlet velocity will increase by 22.24%, 27.8%, and 14.23%, respectively.

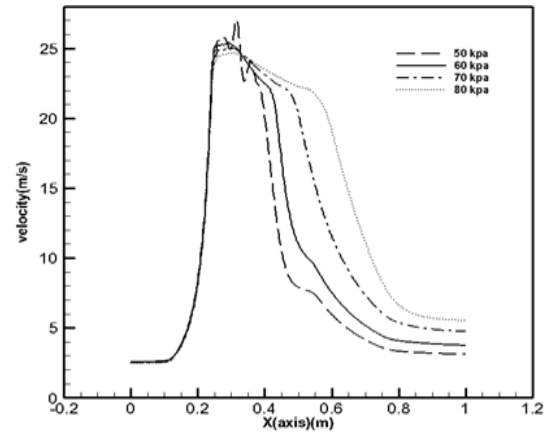


Figure 9. Air inlet pressure effect on the axial velocity along with the ejector

Table 4 illustrates through increasing suction secondary fluid pressure from 50 to 60, 60 to 70, and 70 to 80 kPa, the ejector flow rate ratio increases by 42.83%, 9.38%, and 94.9% respectively. Additionally, by the secondary fluid pressure increase from 50 to 60, 60 to 70, and 70 to 80 kPa, the minimum created pressure for suction increases by 30.11%, 13.99%, and 14.22%, respectively.

Again from Table 2, simulations of 9 to 12, consider the output pressure impact on the ejectors inside flow. Figure 10 depicts the ejector outlet pressure effect on the water and air phase distribution. The air momentum amount decreases through the ejector outlet pressure increase. Thus, its penetration power into the primary fluid of water also decreases. This reduction affects the air and water phase distribution along the axis. The water phase amount will increase by increasing pressure along the axis. Moreover, the dispersion of the water primary layer will decrease, and its continuity increases.

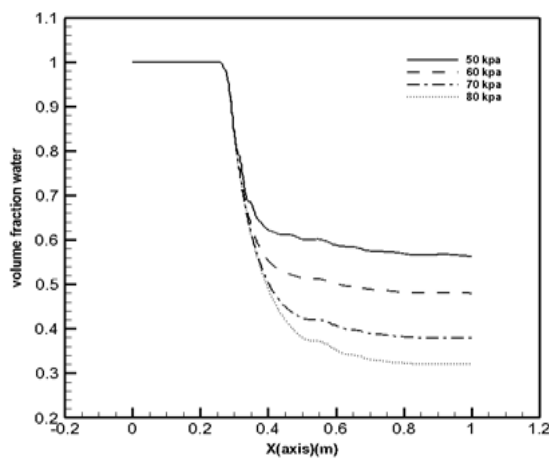


Figure 10. Inlet air pressure effect on the water phase distribution along with the ejector

TABLE 4. Flow rate ratios in different parameters

Parameter	Value	Flow rate ratio
Water inlet pressure (kPa)	390	1.0761
	400	1.2394
	410	1.4831
	420	1.6809
Air inlet pressure (kPa)	50	0.8677
	60	1.2394
	70	1.3557
	80	2.6423
Ejector Outlet pressure (kPa)	130	2.1472
	140	1.2394
	150	0.6646
	155	0
Throat radius (mm)	19	1.6952
	19.5	1.5534
	20	1.2394
	2.5	1.2434
	21	0.9067
Nozzle exit radius (mm)	7	0.7835
	7.5	0
	8	1.2394
	8.5	1.7424
	9	1.9473

The presence of the air phase inside the water layer will gradually decrease as axial distance increases.

As can be noticed, the phases' turbulence has increased at the pressure of 150 kPa, at the ejector's end. This pressure has reached zero after a further increase of the outlet pressure of air suction. After this pressure increase, there would be a back-flow. In other words, instead of suction, the water exits, and it has been observed that there is only the water phase at a pressure of 160 kPa on the symmetry axis. According to Figure 10, through the ejector outlet pressure increase from 130 to 140kPa, from 140 to 150kPa, and from 150 to 160 kPa, the water volume fraction in the ejector output has increased by 32.65%, 18.63%, and 75.31%, respectively. As the ejector's outlet pressure increases, the fluid velocity decreases along the ejector. This causes the mixing percentage of the two fluids of the flow to reduce. Therefore, the water volume fraction increases, and the air volume fraction decreases by increasing the ejector's outlet pressure.

In Figure 11, the water velocity distribution has shown at different outlet pressures. As the pressure increases, the primary fluid velocity decreases. Thus, it has a lower momentum at the output. As the ejector output pressure increases from 130 to 140kPa, 140 to 150kPa, and from 150 to 160 kPa, the velocity at the ejector output is decreased by 26.36%, 23.87%, and

52.79%, respectively. If the discharge pressure increases and exceeds the breaking point's pressure, a back-flow will be generated. In other words, the fluid exits the ejector instead of entering through the secondary inlet.

It can also be seen in Table 4, that by increasing the ejector outlet pressure, the air inlet amount decreases, and the primary fluid energy will be more dissipated for making the secondary fluid entry. Moreover, the air and water fluids will move with lower velocity. As the ejector outlet pressure increases from 130 to 140kPa, 140 to 150kPa, and from 150 to 160 kPa, the flow rate ratio is decreased by 42.27%, 46.37%, and 100%, respectively, and the symmetry axis pressure increases through outlet pressure increase. In Figure 12, the water inlet pressure effect on the air and water phases' distribution has demonstrated (in Table 2-Simulations 1 to 4). Furthermore, the axial velocity in the air-water ejector increases as the water inlet pressure increases. Increasing the inlet pressure causes more pressure drop at the primary nozzle's end.

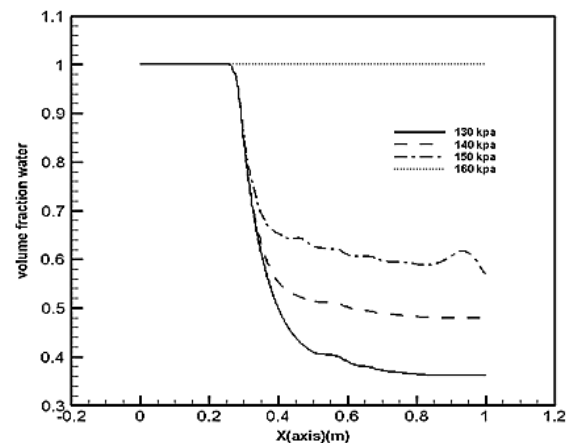


Figure 11. Ejector outlet pressure effect on water phase distribution along the axis

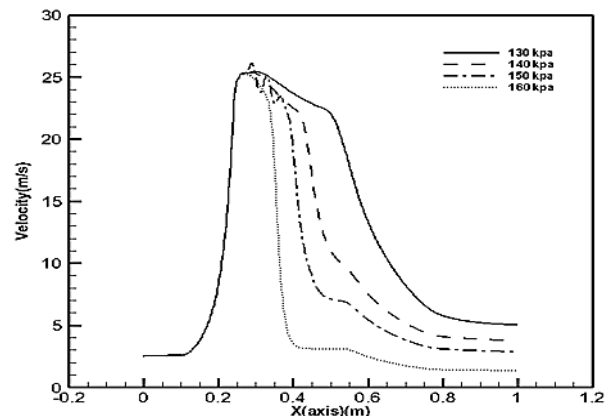


Figure 12. Outlet pressure effect on the axial velocity along the ejector axis

Additionally, the nozzle fundamentally increases the velocity and decreases the pressure. Therefore, it produces a greater vacuum; consequently, the ejector sucks a greater amount of fluid. By water inlet pressure increase, the water phase amount represents a decreasing trend, while the air phase amount indicates an increasing trend.

According to Figure 13, water inlet pressure is increased from 390 to 400kPa, 400 to 410kPa, and from 410 to 420 kPa, causing the water volume fraction at the ejector's end to decrease by 7.28%, 8.76%, and 6.72%, respectively. The fluid velocity increases by increasing the water inlet pressure. This point increases the mixing percentage of the two fluids of the flow. For this reason, the water volume fraction decreases, and the air volume fraction increases by increasing the water inlet pressure.

Now water inlet pressure increases from 390 to 400kPa, 400 to 410kPa, and from 410 to 420 kPa, causing the flow rate to be increased by 15.17%, 19.66%, and 13.33%, respectively. If the water inlet pressure increases, the axial velocity will also increase. In Figure 14, the inlet pressure impact on the velocity distribution has displayed. As can be noted in this figure, the axial velocity in the ejector will increase by increasing the water inlet pressure. This pressure increase has a more significant impact on the velocity after passing through the nozzle. Moreover, it increases the output velocity of the ejector. Additionally, through a more significant velocity increase, the created vacuum will increase that will cause the air suction to enhance. Water inlet pressure increase from 390 to 400, 400 to 410, and from 410 to 420 kPa, causing the velocity at the ejector output to be increased by 9.38%, 12.8%, and 6.33%, respectively.

Figure 15 presents the throat radius impact on the air and water phases in the symmetry axis. As shown in this figure, the flow ratio decreases by increasing the ejector throat radius. As previously mentioned, the secondary

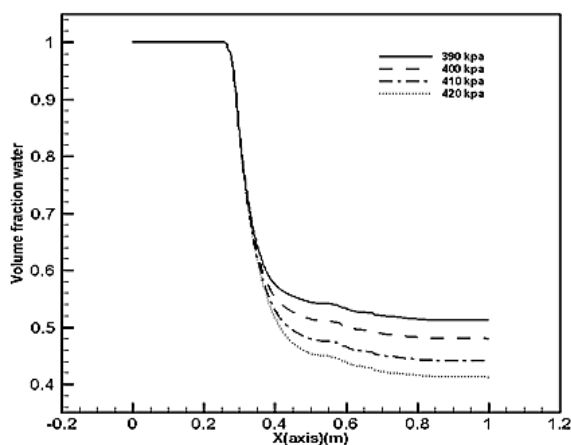


Figure 13. Ejector water inlet pressure impact on water phase distribution along the axis

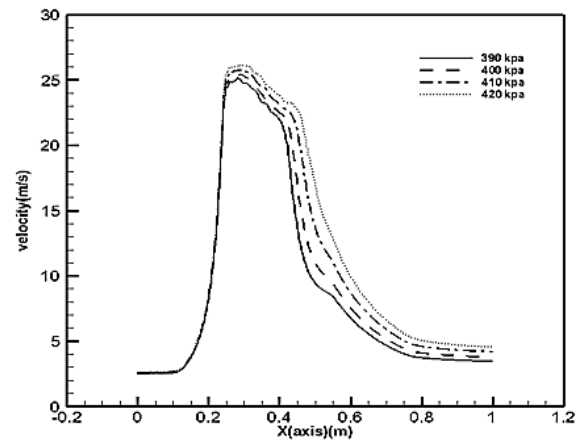


Figure 14. Water inlet pressure effect on the velocity along with the ejector

fluid water is drawn into the ejector due to the working fluid's vacuum and velocity. Moreover, as the throat cross-sectional area increases, a lower amount of fluid is sucked due to pressure increase. The ejector throat radius increases from 19 to 19.5mm and from 19.5 to 20mm, causing the ejector suction to decrease by 8.36% and 20.21%, respectively. However, by increasing the radius from 20 to 20.5 mm, the flow rate ratio increased by 0.3%. Nevertheless, in the case of radius increase from 20.5 to 21 mm, the flow rate ratio decreased by 27.07%. Therefore, the throat radius increase will lead to a volume fraction increase of the water phase in the ejector and result in the air volume fraction decrease. The reason for this point is the pressure increase since by increasing the pressure at the primary nozzle exit, the amount of air suction amount decreased. As we can be seen, a critical state is created at 21 mm, causing inconsistency and oscillation in the air and water phases. According to Figure 16, the ejector throat radius increases results in the velocity reduction in the ejector axis. This velocity decrease contributes to the air suction reduction. The inside behavior of the ejector can be appropriately observed in the contours of Figure 16. It can be noted, the momentum penetration impression on the front layers decreases by increasing the radius. Moreover, the radius increase causes the partial vacuum at the primary nozzle exit to be reduced, while that area's pressure increases.

In Figure 17, the fluid flow vector has been illustrated. As can be noted, increasing the throat radius at the outlet section will cause vortices. Created vortices will generate a resistance barrier, which is one of the reasons for the suction reduction. Considering that the air density is significantly lower than water density, the air momentum has entirely overcome these vortices. Now considering Table 2 simulations of 18 to 22, the water volume fraction in the ejector's central axis is shown in Figure 18.

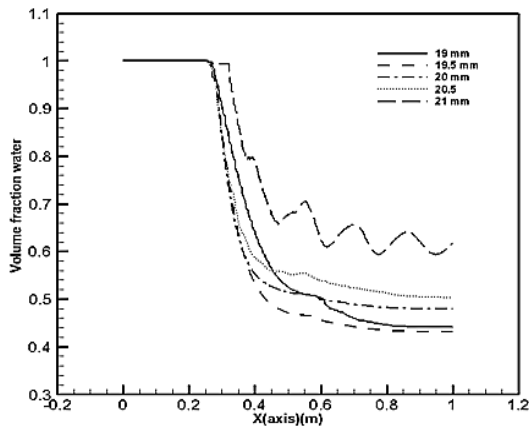


Figure 15. Throat radius on the water volume fraction

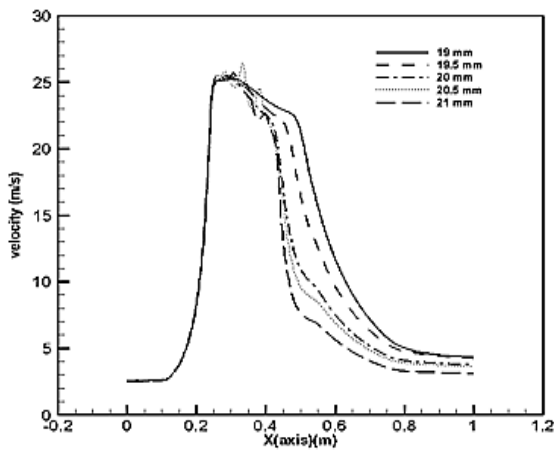


Figure 16. Throat radius impact on the velocity in the ejector

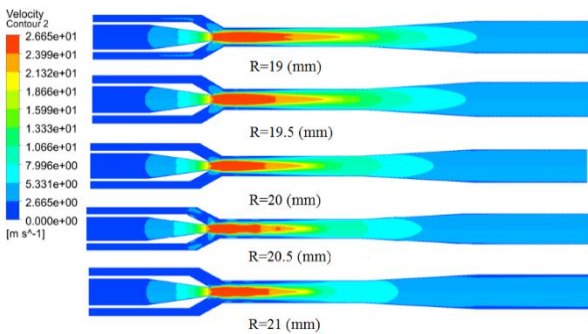


Figure 17. Velocity contour in various throat radius

As shown in Figure 19, increasing the radius of the ejector nozzle exit from 7 to 7.5 mm, from 7.5 to 8 mm, from 8 to 8.5 mm, and from 8.5 to 9 mm, respectively, leads to the reduction of the flow rate ratio by 100% (reaches zero), afterward, increases from zero to 1.23; subsequently, increasing by 40%, and 20.49%. Moreover, as the distance increases, the volume fraction of water decreases, and the air volume fraction increases.

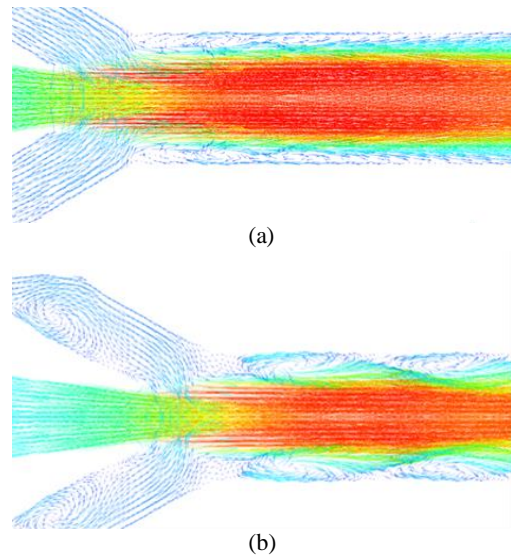


Figure 18. Fluid behavior within the ejector at throat radius of a) 19.5 (mm) b) 20.5 (mm)

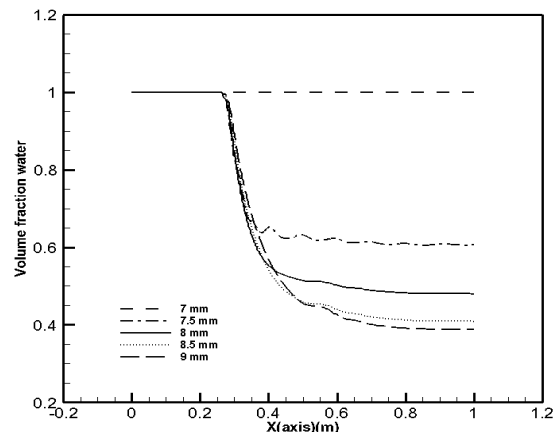


Figure 19. Fluid behavior within the ejector at throat radius of 20.5 (mm)

Figure 20 represents the velocity contour of the cases mentioned above. The radius increase will result in the velocity, and the suction rate increases.

It can be seen from Figure 21 that the velocity increases along with the ejector too. Furthermore, increasing the radius from 7 to 7.5, from 7.5 to 8, from 8 to 8.5, and from 8.5 to 9 mm, leads to enhancement of the velocity at the outlet by 155.29%, 46.51%, 30.53%, and 18.7%, respectively. Additionally, the velocity at the inlet is increased by 14.98%, 15.21%, 15.09%, and 11.46%, respectively. Moreover, by increasing the nozzle radius, the partial vacuum increases, and the air suction amount will increase, as well. Therefore, as discussed in this study, increasing air and water inlet pressure, the flow rate ratio increases. Moreover, by increasing ejector outlet pressure, the flow rate ratio decreases.

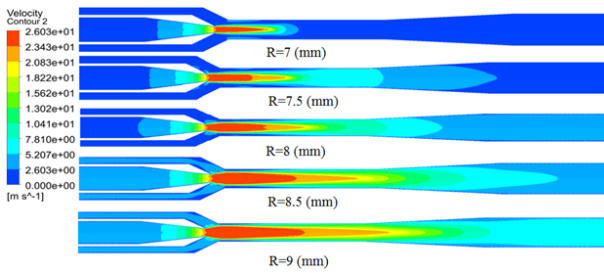


Figure 20. Velocity contour in various throat radius

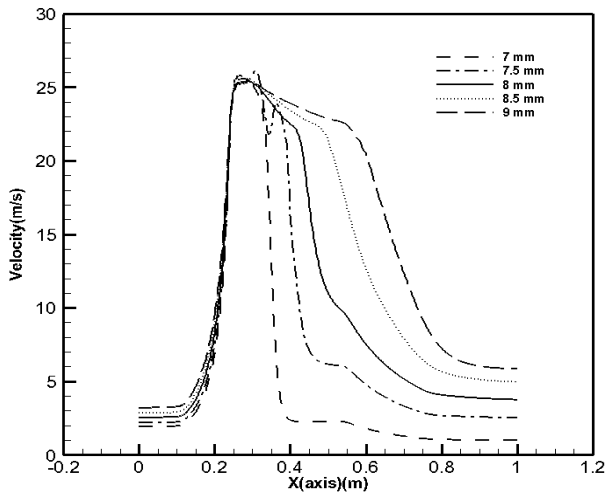


Figure 21. Impact of various ejector nozzle radius on velocity

Further, as the nozzle outlet radius and the ejector throat radius increase, the flow rate ratio increases and decreases, respectively.

5. CONCLUSION

A mixture model and Eulerian-Eulerian two-phase simulation were performed for gas-liquid jet study. Mixture method indicated better, friendlier, and an efficient rather than Eulerian-Eulerian method by comparing to experimental and numerical reported research. Therefore, mixture model was used for parametric study. Results demonstrated that the flow rate ratio increases by increasing the air and water inlet pressure, and by increasing the outlet pressure, the ejector flow rate ratio decreases. In this liquid ejector, unlike the steam ejector, the ejector's flow rate has decreased by increasing the throat's cross-sectional area. The optimal throat radius is considered 20 mm in this study, since it led to the highest flow rate ratio. Additionally, the flow rate increased by increasing the nozzle exit area's radius. The flow rate ratio was increased by 94% by increasing the air inlet pressure from 70 to 80 kPa. Moreover, by increasing the outlet pressure of the liquid ejector, the flow rate decreased. No suction was observed at 160kPa pressure; more specifically, the flow rate was reduced by almost 100% at a pressure of 150 kPa.

6. APPENDIX

TABLE A. Governing equations of this study

Definition	Equations of the Mixture model [25]
Continuity	$\frac{\partial \rho}{\partial t} + \frac{\partial \rho u_i}{\partial x_i} = 0$
Momentum	$\frac{\partial \rho u_i}{\partial t} + \frac{\partial \rho u_i u_j}{\partial x_j} = -\frac{\partial p}{\partial x_i} + \frac{\partial \tau_{ij}}{\partial x_j}$
Stress	$\tau_{ij} = \mu_{eff} \left(\frac{\partial u_i}{\partial x_j} + \frac{\partial u_j}{\partial x_i} \right) - \frac{2}{3} \mu_{eff} \frac{\partial u_k}{\partial x_k} \delta_{ij}$
Density	$\rho = \sum_{k=1}^k \alpha_k \rho_k$
Phases	$\sum_{k=1}^k \alpha_k \rho_k = 1$
Reynolds stress	$-\rho \overline{u_i' u_j'} = \mu_t \left(\frac{\partial u_i}{\partial x_j} + \frac{\partial u_j}{\partial x_i} \right) - \frac{2}{3} \left(\rho k + \mu_t \frac{\delta u_i}{\delta x_i} \right) \delta_{ij}$
Realizable k-ε model k equation	$\frac{\partial \rho k}{\partial t} + \frac{\partial \rho k u_j}{\partial x_j} = \frac{\partial}{\partial x_j} \left(\left(\mu + \frac{\mu_t}{\sigma_k} \right) \frac{\partial k}{\partial x_j} \right) + G_k + G_b + \rho \epsilon - Y_M + S_k$

Realizable k-ε model ε equation	$\frac{\partial \rho \varepsilon}{\partial t} + \frac{\partial \rho \varepsilon u_j}{\partial x_j} = \frac{\partial \left(\left(\mu + \frac{\mu_t}{\sigma_k} \right) \frac{\partial k}{\partial x_j} \right)}{\partial x_j} + \rho C_1 S_\varepsilon - \frac{\rho C_2 \varepsilon^2}{K + \sqrt{v \varepsilon}} + \frac{C_{1\varepsilon} \varepsilon}{K C_{3\varepsilon} G_b} + S_\varepsilon$
Coefficient	$C_1 = \text{Max} \left(0.43, \frac{\mu}{n+5} \right) \quad n = \frac{sk}{\varepsilon} \quad S = \sqrt{2 S_{ij} S_{ij}}$
Equations of Eulerian-Eulerian model [23]	
Continuity	$\frac{\partial (\alpha_k \rho)}{\partial t} + \nabla \cdot (\alpha_k \rho u_k) = 0$
Momentum	$\frac{\partial (\alpha_k \rho u_k)}{\partial t} + \nabla \cdot (\alpha_k \rho u_k u_k) = -\alpha_k \nabla p + \nabla \cdot \tau_k$
Reynolds stress	$-\overline{\rho u_i' u_j'} = \mu_t \left(\frac{\partial u_i}{\partial x_j} + \frac{\partial u_j}{\partial x_i} \right) - \frac{2}{3} \left(\rho k + \mu_t \frac{\delta u_i}{\delta x_i} \right) \delta$
Realizable k-ε model, k equation	$\frac{\partial \rho k}{\partial t} + \frac{\partial \rho k u_j}{\partial x_j} = \frac{\partial \left(\left(\mu + \frac{\mu_t}{\sigma_k} \right) \frac{\partial k}{\partial x_j} \right)}{\partial x_j} + G_k + G_b + \rho \varepsilon - Y_M + S_k$
Realizable k-ε model, ε equation	$\frac{\partial \rho \varepsilon}{\partial t} + \frac{\partial \rho \varepsilon u_j}{\partial x_j} = \frac{\partial \left(\left(\mu + \frac{\mu_t}{\sigma_k} \right) \frac{\partial k}{\partial x_j} \right)}{\partial x_j} + \rho C_1 S_\varepsilon - \frac{\rho C_2 \varepsilon^2}{K + \sqrt{v \varepsilon}} + \frac{C_{1\varepsilon} \varepsilon}{K C_{3\varepsilon} G_b} + S_\varepsilon$
Density relation	$\rho = \sum_{k=1}^k \alpha_k \rho_k$
Phases	$\sum_{k=1}^k \alpha_k \rho_k = 1$

7. REFERENCES

1. Bagheri-Esfe, H. and Dehghan Manshadi, M., "A low cost numerical simulation of a supersonic wind-tunnel design", *International Journal of Engineering, Transactions A: Basics*, Vol. 31, No. 1, (2018), 128-135. doi: 10.5829/ije.2018.31.01a.18
2. Aminoroayaie Yamini, O., Mousavi, S.H., Kavianpour, M. and Safari Ghaleh, R., "Hydrodynamic performance and cavitation analysis in bottom outlets of dam using cfd modelling", *Advances in Civil Engineering*, Vol. 2021, (2021). Article ID 5529792, doi.org/10.1155/2021/5529792
3. Mousavimehr, S., Yamini, O.A. and Kavianpour, M., "Performance assessment of shockwaves of chute spillways in large dams", *Shock and Vibration*, Vol. 2021, (2021). Article ID 6634086, doi.org/10.1155/2021/6634086
4. Movahedi, A., Kavianpour, M. and Aminoroayaie Yamini, O., "Experimental and numerical analysis of the scour profile downstream of flip bucket with change in bed material size", *ISH Journal of Hydraulic Engineering*, Vol. 25, No. 2, (2019), 188-202. doi.org/10.1080/09715010.2017.1398111
5. Khatamnejad, H., Khalilarya, S., Jafamadar, S., Mirsalim, M. and Dahodwala, M., "Toward an improvement of natural gas-diesel dual fuel engine operation at part load condition by detail cfd simulation", *International Journal of Engineering Transactions A: Basics*, Vol. 31, No. 7, (2018), 1082-1087. doi: 10.5829/ije.2018.31.07a.11
6. Shiravi, A.H., Firoozzadeh, M. and Lotfi, M., "Experimental study on the effects of air blowing and irradiance intensity on the performance of photovoltaic modules, using central composite design", *Energy*, Vol. 238, Part A, (2022), 121633. doi.org/10.1016/j.energy.2021.121633
7. Azizi, K. and Keshavarz Moraveji, M., "Computational fluid dynamic-two fluid model study of gas-solid heat transfer in a riser with various inclination angles", *International Journal of Engineering, Transactions A: Basics*, Vol. 30, No. 4, (2017), 464-472. doi: 10.5829/idosi.ije.2017.30.04a.02
8. Shiravi, A.H., Shafiee, M., Firoozzadeh, M., Bostani, H. and Bozorgmehrian, M., "Experimental study on convective heat transfer and entropy generation of carbon black nanofluid turbulent flow in a helical coiled heat exchanger", *Thermal Analysis and Calorimetry*, Vol. 145, No. 2, (2021), 597-607. doi.org/10.1007/s10973-020-09729-1
9. Hasanpour, B., Irandost, M., Hassani, M. and Kouhikamali, R., "Numerical investigation of saturated upward flow boiling of water in a vertical tube using vof model: Effect of different boundary conditions", *Heat and Mass Transfer*, Vol. 54, No. 7, (2018), 1925-1936. doi.org/10.1007/s00231-018-2289-3
10. Khan, R., "Numerical investigation of the influence of sand particle concentration on long radius elbow erosion for liquid-solid flow", *International Journal of Engineering Transactions A: Basics*, Vol. 32, No. 10, (2019), 1485-1490. doi: 10.5829/ije.2019.32.10a.18
11. Torfeh, S. and Kouhikamali, R., "Numerical study of different gas-solid flow regimes effects on hydrodynamics and heat

- transfer performance of a fluidized bed reactor", *Heat Transfer—Asian Research*, Vol. 49, No. 1, (2020), 213-235. doi.org/10.1002/hjt.21607
12. Keenan, J.H., Neumann, E.P. and Lustwerk, F., "Investigation of ejector design by analysis and experiment", *Journal of Applied Mechanics*, (1950) 299-309.
 13. D. Sharma, P., A., Ranade, V., "Effect of turbulent dispersion on hydrodynamic characteristics in a liquid jet ejector," *Energy*, Vol. 164, (2018) 10-20. doi.org/10.1016/j.energy.2018.08.171
 14. K. Pianthong, S., W., Behnia, M., Sriveerakul, T., Aphomratana, Senthil Kumar, R., Kumaraswamy, S., Mani, A., "Investigation and improvement of ejector refrigeration system using computational fluid dynamics technique ", *Energy Conversion and Management*, Vol. 48, No. 9 (2007), 2556-2564. doi.org/10.1016/j.enconman.2007.03.021
 15. P. Cramers, B., A., "Influence of the ejector configuration, scale and the gas density on the mass transfer characteristics of gas-liquid ejectors". *Chemical Engineering Journal*, Vol. 82, No. 1-3 (2001): 131-141. doi.org/10.1016/S1385-8947(00)00363-6
 16. R. Senthil Kumar, K., S., Mani, A., "Experimental investigations on a two-phase jet pump used in desalination systems", *Desalination*, Vol. 204, No. 1-3, (2007), 437-447. doi.org/10.1016/j.desal.2006.03.546
 17. Jafarnadar, S., "The effects of pressure difference in nozzle's two phase flow on the quality of exhaust mixture", *International Journal of Engineering, Transactions B: Applications*, Vol. 26, No. 5, (2013), 553-562. doi: 10.5829/idosi.ije.2013.26.05b.12
 18. Zhu, P.J.Y., "Bypass ejector with an annular cavity in the nozzle wall to increase the entrainment: Experimental and numerical validation", *Energy*, Vol. 68, (2014), 174-181. doi.org/10.1016/j.energy.2014.02.046
 19. W.C. Y. Zhu, C.W., Y. Li, "Numerical investigation of geometry parameters for design of high performance ejectors", *Applied Thermal Engineering*, Vol. 29, No. 5-6, (2009): 898-905. doi.org/10.1016/j.applthermaleng.2008.04.025
 20. J.Y. D. Chong, G.W., J. Liu, "Structural optimization and experimental investigation of supersonic ejectors for boosting low pressure natural gas", *Applied Thermal Engineering*, Vol. 29, No. 14-15, (2009), 2799-2807. doi.org/10.1016/j.applthermaleng.2009.01.014
 21. Kouhikamali.R., N. Sharifi, "Experience of modification of thermo-compressors in multiple effects desalination plants in assaluyeh in iran", *Applied Thermal Engineering*, Vol. 40, (2012), 174-180. doi.org/10.1016/j.applthermaleng.2012.02.002
 22. J.Y. L. Wang, C.W., X. Li, "Numerical study on optimization of ejector primary nozzle geometries", *International Journal of Refrigeration*, Vol. 76, (2017), 219-229. doi.org/10.1016/j.ijrefrig.2017.02.010
 23. Bhutada, S.R., Pangarkar, V.G., "Gas induction and hold-up characteristics of liquid jet loop reactors", *Chemical Engineering Communications*, Vol. 61, No. 1-6, (1987), 239-258. doi.org/10.1080/00986448708912041
 24. Wang, X., Chen, Y., Li, M., Xu, Y., Wang, B. and Dang, X., "Numerical investigation of the cavitation performance of annular jet pumps with different profiles of suction chamber and throat inlet", *Engineering Applications of Computational Fluid Mechanics*, Vol. 14, No. 1, (2020), 1416-1428. doi.org/10.1080/19942060.2020.1824875
 25. H.L. Xiaodong Wang, J.D., Jiaqi Wu, Ji-yuan Tu, "Numerical study on mixing flow behavior in gas-liquid ejector", *Experimental and Computational Multiphase Flow*, Vol. 3, (2021), 108-112. doi.org/10.1007/s42757-020-0069-z

Persian Abstract

چکیده

در این تحقیق، مخلوط حالت پایدار و روش Eulerian-Eulerian برای خارج کننده جریان موازی گاز مایع-گاز مورد بررسی قرار گرفت. شبیه سازی نشان داد که شبیه سازی مدل مخلوط نشان دهنده بهتر و کارآمدتر است. مدل Eulerian-Eulerian به زمان محاسباتی طولانی تری نیاز داشت و برای دستیابی به همگرایی مطلوب دارای پیچیدگی بود. با این حال، عملکرد هر دو روش کمی مشابه نشان داده شد. مدل ها اختلاف حدود ۶ درصد را در نسبت جریان نشان دادند، نمودارهای فشار آنها تقریباً منطبق است و پارامتر سرعت آنها در مقایسه با داده های تجربی موجود ۷ درصد متغیر است. علاوه بر این، نتایج مدل مخلوط بسیار بهتر با داده های تجربی مطابقت دارد. بنابراین، مدل مخلوط برای مطالعه پارامتری بعدی انتخاب شد. نتایج شبیه سازی نشان داد که نسبت دبی با افزایش سطح مقطع گلو کاهش می یابد و نسبت جریان با افزایش سطح مقطع نازل افزایش می یابد. در این رابطه، به عنوان مثال، نسبت دبی خروجی با افزایش فشار از ۷۰ به ۸۰ کیلو پاسکال، ورودی هوا تا ۹۴ درصد افزایش می یابد، و با افزایش فشار خروجی خروجی، نسبت جریان کاهش می یابد به طوری که هیچ مکشی در آن مشاهده نمی شود. ۱۶۰ کیلو پاسکال در نتیجه، در نسبت فشار ۱۵۰ کیلو پاسکال، نسبت جریان تقریباً ۱۰۰ کاهش یافت.
